ADVANCED MATERIALS INTERFACES
Open Access
www.advmatinterfaces.de

Stable Air Retention under Water on Artificial Salvinia Surfaces Enabled by the Air Spring Effect: The Importance of Geometrical and Surface-Energy Barriers, and of the Air Spring Height

Lutz Speichermann-Jägel, Susanna Dullenkopf-Beck, Robert Droll, Daniel Gandyra, Matthias Barczewski, Stefan Walheim, and Thomas Schimmel*

Superhydrophobic surfaces that can remain dry under water have a high potential as nontoxic antifouling coatings or for drag-reducing ship coatings. The Salvinia effect leads to impressive stable air layers on underwater submerged floating plants *Salvinia*, decisively determined by the hydrophilic tips of the otherwise hydrophobic *Salvinia* hairs (Salvinia paradox). The water adheres to these hydrophilic tips, stabilizing the water–air interface. An even more important contribution to the stability of the air layer is provided by the air spring, which is formed by the air volume bound by the hydrophilic leaf edge and the leaf base. Using an artificial Salvinia model with hydrophobic pillars (syn-trichomes), how the stability against pressure changes in water depends on the height of the artificial hair is systematically shown: a reduction of the air spring height from 3 mm to 300 µm increases the stability against negative pressure by 500% from 72 to 380 mbar. Thicker air layers react much more strongly when subjected to overpressure (1000 mbar). It is also shown that the presence of a boundary is essential for the function of the air spring: removing the limiting hydrophilic edge around the hydrophobic air spring reduces the stability against negative pressure by 300%.

1. Introduction

The floating fern *Salvinia molesta* can hold air under water for any length of time on its superhydrophobic/aerophilic upper leaf surface, which is covered with complex, egg-beater-like hairs, and thus breathe under water.[1] Inspired by this role model, numerous attempts have been made in the last decade to 1) understand the phenomenon and 2) produce artificial, micro- and nanostructured surfaces that hold air underwater.

This quest is mainly driven by the prospect of technical surfaces that remain dry under water forever, which could solve the fouling problem in shipping, or, e.g., aquafarming, or floating installations such as solar parks, without using toxic antifouling paints. The ultimate goal would be a coating that simultaneously reduces the friction of the ship's hull against the water or during fluid transport in channels or pipelines through air lubrication. Air retention extends the field of applications of superhydrophobic surfaces as self-cleaning and water-repellent surface.[2–12]

It has already been shown that superhydrophobic, air-retaining surfaces have an immense potential for drag reduction[13–20] (25%),[21] or the slip length of the hydrodynamic velocity profile as a corresponding quantity,[22–27] both under laminar and turbulent conditions,[28,29] or in fluid

L. Speichermann-Jägel, S. Dullenkopf-Beck, R. Droll, D. Gandyra, M. Barczewski, S. Walheim, T. Schimmel
Institute of Nanotechnology (INT)
Karlsruhe Institute of Technology
Herrmann-von-Helmholtz-Platz 1, D-76344 Eggenstein-Leopoldshafen, Germany
E-mail: stefan.walheim@kit.edu

The ORCID identification number(s) for the author(s) of this article can be found under https://doi.org/10.1002/admi.202400400

DOI: 10.1002/admi.202400400

L. Speichermann-Jägel, S. Dullenkopf-Beck, R. Droll, D. Gandyra, M. Barczewski, S. Walheim, T. Schimmel
Institute of Applied Physics (APH)
Karlsruhe Institute of Technology
Wolfgang-Gaede-Str. 1, D-76131 Karlsruhe, Germany

S. Walheim
Karlsruhe Nano Micro Facility (KNMFi)
Karlsruhe Institute of Technology
Herrmann-von-Helmholtz-Platz 1, D-76344 Eggenstein-Leopoldshafen, Germany

T. Schimmel
Materials Research Center for Energy Systems (MZE)
Karlsruhe Institute of Technology
Straße am Forum 7, D-76131 Karlsruhe, Germany

transport and even in prototypical, experimental hull coatings,[22,30–34] which have already been produced and applied to very large areas.[35]

However, these promising underwater applications depend on the long-term stability of the underwater air layers,[20,36–43] which has not yet been achieved. Some contributing factors have been investigated, such as the relationship between structure size, surface chemistry, and maximum immersion depth:[42–45] The structure size must be as small as possible and the material as hydrophobic as possible to retain air deep underwater.[44–46] Further investigated contributing factors are the gas saturation of the surrounding liquid, due to the possibility of air loss through the occurring diffusion between gas layer and water,[47] For all gases there exists a minimum pore size where indefinite lifetime is achievable, which depends on both geometry and gas saturation.[48]

The floating fern *Salvinia molesta* is a well-studied species that exhibits the ability to retain air with an infinite lifetime, which therefore makes it THE biological role model[31,49–58] with various approaches being taken to mimic its structure and functionality.[15,44,59–63]

Based on the observation of air retention of floating ferns, five criteria for permanent air retention were recognized early on:[36] 1) hydrophobic chemistry, 2) nanostructured topography, 3) hierarchical architecture, 4) overhanging structures and 5) the elasticity of the hairs (trichomes). All these features are realized on the upper surface of *Salvinia* leaves by a covering of the upper leaf surface with elastic, egg beater-like trichomes (**Figure 1**), whose aerophilic surfaces are coated with superhydrophobic, nm-sized wax crystals that prevent the penetration of water. *Salvinia molesta*, together with some of its relatives, has another remarkable detail: The wax crystals are missing at the tips of the trichomes, making them hydrophilic and thus water-attracting.[64,65] These hydrophilic cells "clamp" the water at the interface and thus stabilize it.[1] The elasticity of the hairs is of great importance for the stability of the air layer under varying pressure conditions, since such circumstances lead to variations in the air layer thickness on the leaf surface, to which the trichomes can adapt by bending or by compression and expansion. When the limit of adaptability is reached, the pinning force of the hydrophilic tips (the so-called apices) helps to stabilize the air layer (the Salvinia paradox).[1] This advantageous property has already been investigated in own publications,[1,66] described theoretically (see, e.g.,)[67] and implemented in artificial model surfaces.[61,68,69] In our earlier work,[1] we were able to show that the air volume enclosed by the hydrophobic film acts like an air spring that counteracts expansion in the event of positive or negative pressure. Overcoming this spring by opening the air volume with an air hose drastically reduced the stability of the air layer.[66] Instead of 60 mbar, the hydrophilic *Salvinia* hairs could only withstand 1% of the negative pressure (still 0.6 mbar) before the air/water interface became unstable and detached from the hair tips. The air spring therefore makes a decisive contribution to stability against pressure variations, which cannot be avoided in turbulent flow.

Here we raise the question to what extent the pinning force of the tips (Salvinia paradox) of the structure contributes to the stability of the air layer of analogous artificial structures under negative pressure and how exactly the stabilizing air spring effect depends on the thickness of the air layer, which in the case of the natural system (*Salvinia molesta*) is about 2.5 mm. In our experiments, we therefore vary the height of the air spring from 300 µm to 3 mm. The importance of the edge is also investigated: Does the presence and configuration of different barrier types, purely geometrical and chemical, influence the behavior of the air spring structures, and can a new design rule for artificial air retaining surfaces be established?

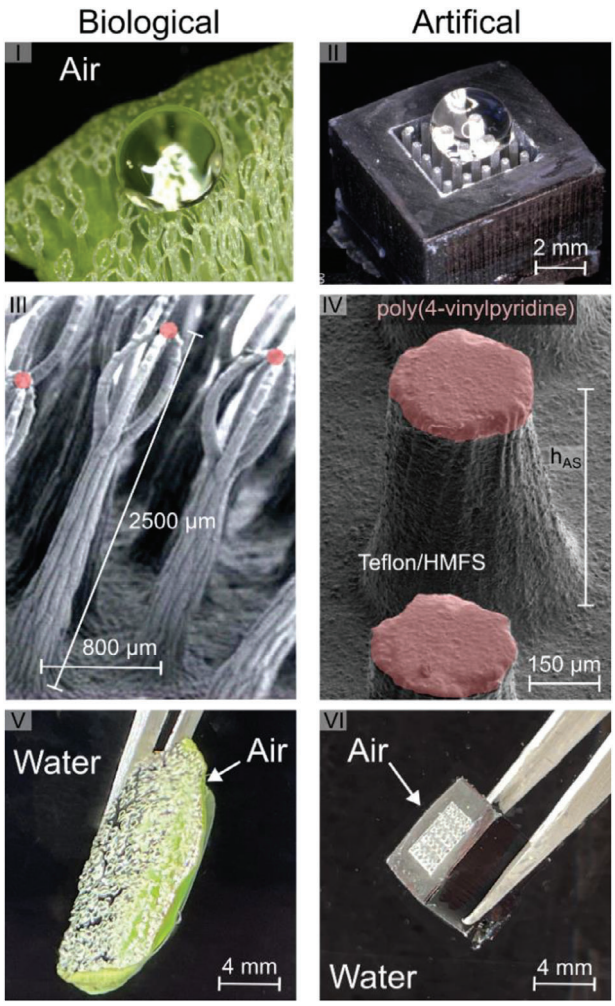

Figure 1. The biological model of stable air retention under water is the floating fern *Salvinia molesta* (I). The floating leaves are covered with hydrophobic hairs (trichomes) that allow water droplets to roll off (I). These trichomes have a complex shape and are covered with nanoscale wax crystals. At their tip they have a hydrophilic spot in the form of four terminal, dead cells. (Marked in red in III, not visible in detail) If the plant is submerged under water, an air cushion forms around the hairs, whose thickness is defined by the length of the hairs (*V*). The hydrophilic tips stabilize the air cushion by holding the air–water interface. Our artificial counterpart of an air-holding structure has the essential features of the biological model: cylindrical rods that are hydrophobically coated, a boundary that is created in the plant by the hydrophilic edge of the leaf (II). The tips of the artificial trichomes (syn-trichomes) are also hydrophilic, which is achieved by a subsequent coating (red in IV). Like the trichomes of the plant, the syn-trichomes stretch a silvery, shiny layer of air under water (VI).

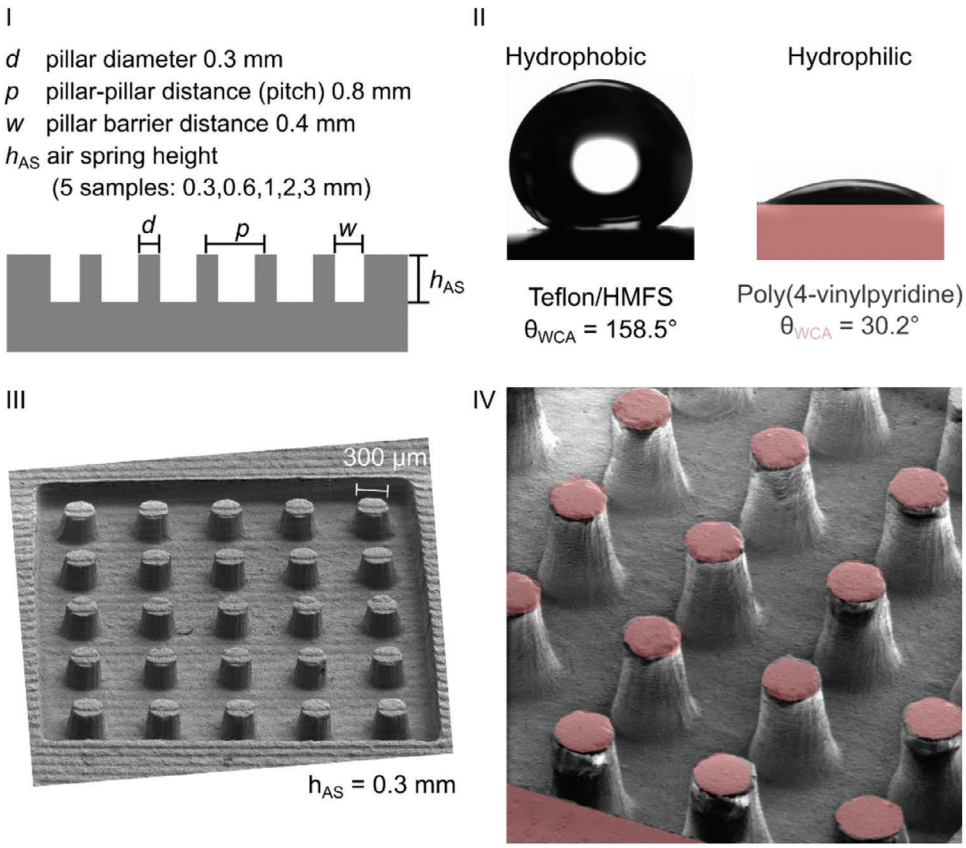

Figure 2. The dimensions of the artificial Salvinia structures are shown in (I). Five sample types with different height of syn-trichomes were produced by 3D printing. The surface energy contrast was achieved by a hydrophobic coating with Teflon/HMFS (static water contact angle 158.5° (II left)) and a selective hydrophilic functionalization of the column tips with poly(4-vinylpyridine) (static water contact angle 30.2° (II right in red—shown in red in the SEM image (IV)). Both the column tips and the edge of the structure were hydrophilically functionalized.

2. Results and Discussion

2.1. Manufacturing of Artificial Salvinia-Like Structures

The investigated structures were templated abstractly after the functional structures of the floating fern *Salvinia molesta*. The complex 3D structure of the floating fern was represented by a simplified 2.5D columnar structure of geometrically similar size. The structures were arranged as bordered groups of 5 × 5 columns, with column diameters of 0.3 mm, a distance of 0.8 mm and a distance to the wall of 0.4 mm (see **Figure 2**). The height of the structures was varied between 0.3 and 3 mm (approximately the height of natural *Salvinia* trichomes), i.e., an aspect ratio between 1 and 10, to investigate the influence of height. Figure 1 shows both the biological model and the artificial structure. The hydrophobic property is immediately apparent when a drop of water is deposited on the upper side of the leaf or the artificial structure. Microscopically, both structures (SEM images II and IV) have a rough surface, which in the case of the plant consists of nanoscale wax crystals and in the case of the artificial structure of a particle-filled Teflon coating. The hydrophilic ends (marked in red) consist of dead cells without a wax coating in the case of the plant and a hydrophilic polymer layer in the case of the artificial structure. When submerged, both the plant (here a halved leaf was submerged) and the artificial structure show an air coat stretched by the trichomes, which can be clearly recognized by the silvery shine arising from the total reflection of light.

The hydrophilic edge of both the plant and the artificial structure appears dark, as no air is held there. The initial structures were produced using 3D printing by stereo lithography and then replicated in epoxy resin. To approximate the surface chemistry of *Salvinia* leaves, the surface was coated with a dispersion of hydrophobically modified fused silica microparticles (HMFS) in a 1wt% solution of Teflon AF in a perfluorinated solvent. The tips of the structure were rendered hydrophilic by a coating of poly-(4-vinyl)pyridine, which was subsequently hardened using an UV light treatment.

2.2. Air Layer Stability on a Submerged Syn-Trichome Structure Studied by LSCM

To assess the air layer persistence, we measured the negative pressure needed to make the first hair tip lose contact with the water: When exposed to an increasing under pressure, the trapped air of a leaf expands, and the air–water interface between the hair tips curves upwards, obtaining a more arch-like shape.[58]

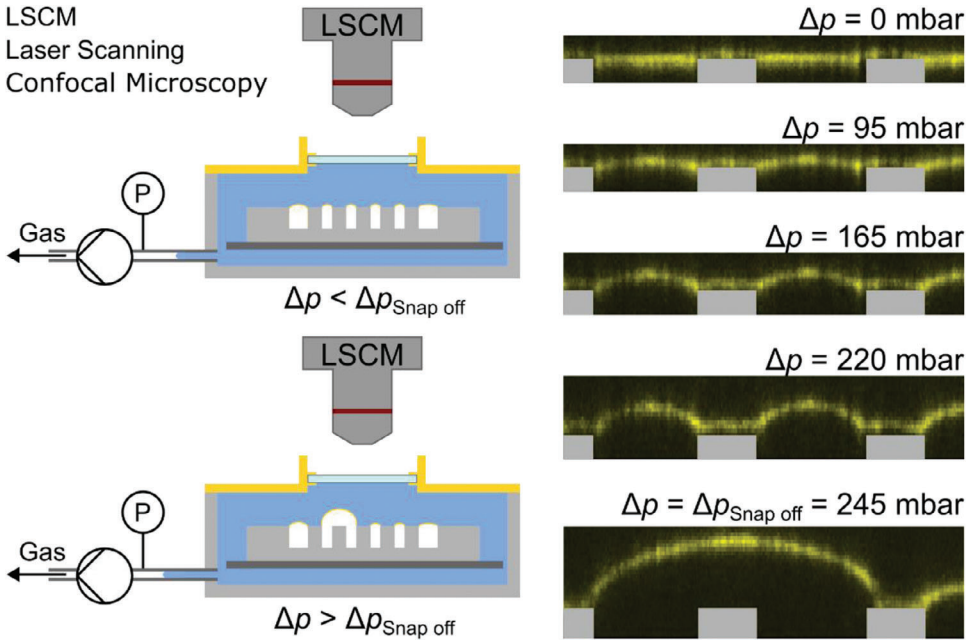

Figure 3. Observation of the air–water-interface shape at varying pressures using laser scanning confocal microscopy (LSCM): To determine the behavior of the entrapped air layer, the submerged samples were exposed to under pressure, using a self-built pressure vessel. The shape of the air volume was imaged using LSCM, whereby the air-water interface was labeled using sedimented, fluorescent particles (yellow). When exposed to an under pressure, the retained air expands and the interface curvature between adjacent pillars increases. At an air-spring-height specific pressure difference (here: 245 mbar to atmospheric), the interface expands to such an extent that it first loses contact with one pillar. This pressure difference we call snap off pressure $\Delta p_{\text{snap off}}$.

We studied this process of meniscus deformation due to under pressure experimentally by using a pressure cell adapted to a laser scanning confocal microscope (LSCM).[41] The air/water interface was fluorescently labelled by staining it with fluorescing pigment particles, which sedimented to the interface. The emitted fluorescence signal from the interface was subsequently detected with the LSCM and could be rendered into a cross section of the interface. The applied pressure difference was incrementally increased and the interface shape determined, until the first loss of contact between water and structure occurred. This was defined as the snap-off pressure difference $\Delta_{\text{snap off}}$ (**Figure 3**). These measurements for every sample were repeated 10 times with this and an adapted setup with optical snap off control.

Two important effects could be observed: The higher the functional structure (syn-trichome), the lower the required snap off pressure difference. This means in negative pressure situations, that lower structures retain air better then otherwise geometrically and chemically identical higher samples. The data in **Figure 4** show that the relationship between structural height and pressure stability follows an $1/h$ proportionality.

Purely hydrophobic samples, when compared to hydrophilic samples, lose contact at much lower pressure differences. This higher stability arises from the mechanical stabilization of the interface through the repeated pinning on top of the pillars. Greater forces, thus higher pressures, are necessary to detach the interface successfully. This stability enhancement we call the "Salvinia enhancement factor E_S", and can be calculated using formula 1.

$$E_S = \frac{\Delta p_{\text{Ssnap off, hydrophil}}}{\Delta p_{\text{Ssnap off, hydrophob}}} \quad (1)$$

Averaged across all investigated samples the mean value of E_S is 1.82, ranging between 1.73 and 2.22, where especially with the higher structural heights the measuring accuracy potentially skews the value.

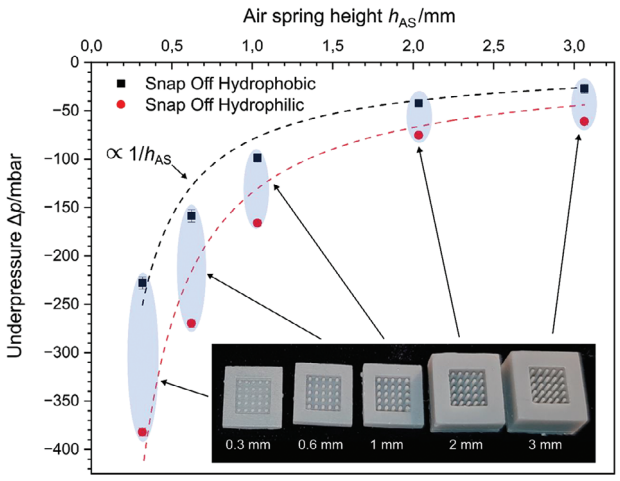

Figure 4. Air spring effect on biomimetic surfaces of different air spring heights: Depending on the height of the air spring, different under pressure to cause the first snap-off are necessary. We find an inverse proportional dependence of $\Delta p_{\text{snap off}}$ to the air spring height defined by the pillar height. When comparing completely hydrophobic, to hydrophilic air springs, a further increase in under pressure stability (Salvinia factor between 1.7 and 2.2) is observable.

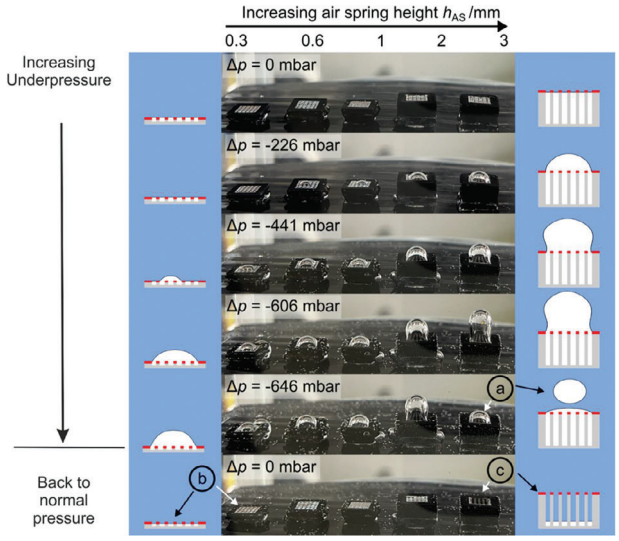

Figure 5. Simultaneous under pressure exposure: When samples with different air spring heights are simultaneously exposed to the same pressure cycle the increasing strength with decreasing thickness of the air spring is obvious: After a pressure reduction down to one third, implying an volume increase to 300%, b) the 0.3 mm spring recovers, while the highest 3 mm air spring shows c) an air loss via a) bubble formation. After the return to atmospheric pressure, the air layer for thin air springs is fully intact (b), whereas the thicker air spring shows an significantly reduced air volume (no visible air layer anymore (c)).

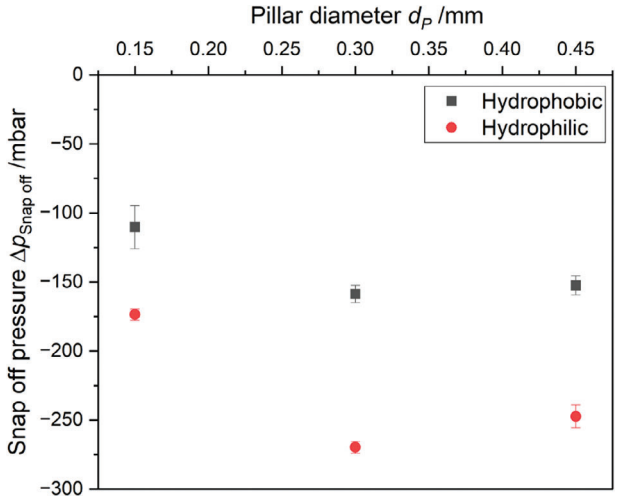

Figure 6. The determined snap off pressure shows a relatively weak correlation with the column diameter, although the achieved negative pressure clearly increases with increasing column diameter. This can be explained, on the one hand, by the increased adhesion of the column heads with increasing diameters, but also by the air spring effect, as the larger column diameters lead to an overall reduction in the retained air volume and thus effectively to a stiffer air spring. The amplification by the hydrophilic (Salvinia-like) column heads (the Salvinia factor) is 1.57 for the thinnest columns (150 µm), 1.70 for the medium columns (300 µm) and 1.61 for the thicker columns (450 µm), i.e., 1.63 on average.

If samples of different structural height are exposed, as seen in **figure** 5, to the same pressure difference, the dependency is clearly visible: The expansion of the air layer increases with increasing construction height. If the pressure difference is high enough, the air can no longer be retained and is lost in the form of bubbles, where the velocity of the air loss is proportional to the height difference, since higher structures, at constant pressure change rate, reach the snap off pressure earlier. This clearly demonstrates the geometric dependency of the air retention.

In addition to the height of the columns, which define the thickness of the air layer, their diameter can also be varied. This parameter should also influence the stability of the air layer, as the adhesion of the enlarged column heads should result in an increase in the snap-off pressure, even if this effect should be less pronounced for column diameters above 100 µm.[66] **Figure 6** shows the negative pressure stability (snap-off pressure as a function of the column diameter). Columns 150, 300, and 450 µm thick were arranged on the previously used grid.

There is indeed an increase in the snap-off pressures with increasing column diameters. However, it must also be borne in mind that the air volume decreases as the column diameter increases, effectively making the air spring stiffer. An increase in the snap-off pressures can be clearly seen with hydrophilic column heads compared to the completely hydrophobic columns (red in Figure 6). The Salvinia factor is 1.63 on average and is very pronounced for all 3 column diameters (1.57 for 150 µm, 1.7 for 300 µm, and 1.61 for 450 µm thick columns).

Now that it is clear that a thicker layer of air reduces the stability of the air holding at negative pressure, it is of course also interesting to consider the situation at positive pressure. Here, too, it is to be expected that a thinner layer of air is less strongly moved by the external pressure. **Figure** 7 summarizes the results of an experiment with a confocal microscope. Here, overpressures of up to one bar could be achieved, which corresponds to a hydrostatic pressure at a water depth of 10 m. The result clearly shows how the air-water interface is compressed by about half. For the thin sample with a column height of 300 µm, this results in a deformation of 150 µm, whereas for 3 mm high columns, these protrude 1500 µm into the water. This shows that the thinner and therefore stiffer the air spring will form a smoother surface with corresponding pressure fluctuations, which will be relevant for the potential use of air layers to reduce friction in hydrodynamic applications.

To investigate the importance of both a geometric barrier (GB) and a surface energy barrier (SEB) for optimum air retention stability, we produced samples with hydrophilic tips with and without a boundary wall. There are four variants: 1) without any boundary (5 × 5 columns free-standing on the hydrophobic surface) 2) the same with a boundary wall, 3) with a hydrophilic wall boundary and 4) without a boundary wall but with a hydrophilic bottom outside the column array.

Under pressure variation experiments show a clear result (**Figure** 8): Both the geometric boundary in the form of the wall and the surface energy limitation in the form of a hydrophilic closure are necessary and the best results can be achieved with a combination of both. The direct analogy to the plant is not readily apparent here, as it has no wall boundary. Here, nature solves the problem through trichomes becoming lower and lower towards the edge, the plant thus drawing the boundary line both to the ground and the hydrophilically functionalized edge. This is technically difficult to implement as it requires a complex,

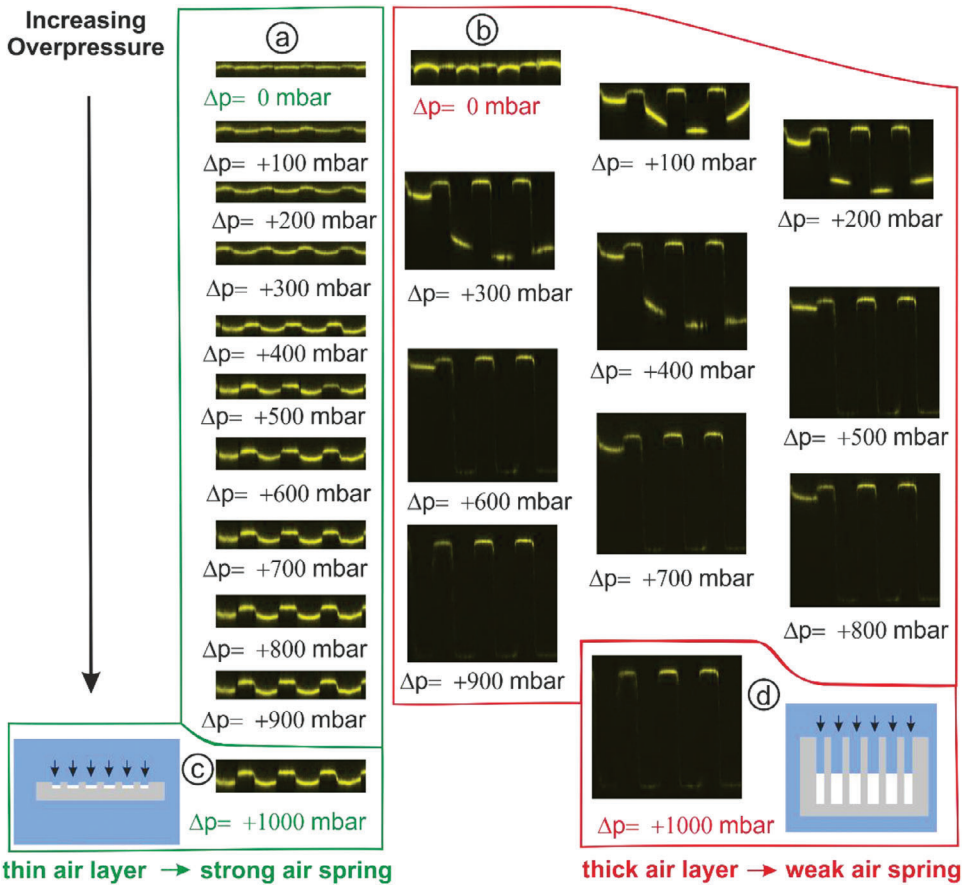

Figure 7. To investigate the effect of air spring thickness in overpressure situations, two samples were exposed to increasing overpressure from 0 mbar to 1000 mbar: one sample with a height of 300 µm (green data) and one with a height of 3000 µm (red data). The air–water interface was imaged using confocal microscopy. The thin air layer is pushed downwards by about 150 µm (situation at (a–c)), while the thick air layer collapses by about 1500 µm (situation at (b–d)). The thicker air layer therefore has a lower restoring force (weaker air spring).

hierarchical structure across several length scales. In addition, for large-area structures the approach of a flat air/water interface with wall crowns and column tips on the same level is more promising than a bowed surface as found on *Salvinia leaves*. The leaves trichomes are longer in the center than at the edge.

3. Conclusions

Artificial structures inspired by *Salvinia* (array of hydrophobic/aerophilic "syn-trichomes" surrounded by geometrical barriers) were successfully created using nature as a model. Using a combination of laser lithography, replication in epoxy resin and coating processes, both purely hydrophobic and mixed hydrophobic/hydrophilic structures were produced. The height of the structures was varied between 0.3 and 3 mm. When such structures are exposed to pressure variations toward under pressure, two important tendencies were observed and quantified: As the pressure difference increases, the air layer bends outwards from the structure and if this difference is large enough, contact between the structure and the interface is lost (snap-off pressure). This snap-off pressure is inversely proportional to the height of the structures, whereby lower structures and thus thinner air layers require much higher pressure differences (10-fold decrease in height, 14-fold increase in pressure) for the snap-off pressure to occur. Hydrophilically functionalized syn-trichome tips stabilize the air layer even more and thereby increase the required pressure difference, with the observed increase in the Salvinia effect between structures of the same height being about twofold (minimum 1.7×, maximum 2.2 (Salvinia Enhancement Factor)). In the case of overpressure loading up to 1 bar (corresponding to 10 m water depths), the hardness of the air spring could also be demonstrated with thin layers of air, whereby 10 times thicker layers of air are depressed correspondingly 10 times deeper.

Finally, we investigated the role of the edge of the structural unit. As with the *Salvinia* leaf, the artificial air retaining structures also have an edge that seals off the air volume and stabilizes the enclosed air layer both geometrically as a wall boundary and through its hydrophilicity. Without this edge seal, the air can escape to the side and be quickly transported away in the form of migrating bubbles, especially in hydrodynamic flow conditions.

These results provide new, additional guidelines (low air layer height/strong air spring and both strong geometric boundary GB and strong surface energy boundary SEB) for the design of truly permanent air retaining structures, which are necessary for a broad adaptation in technical applications. More research is required to quantify further the influences of both geometrical

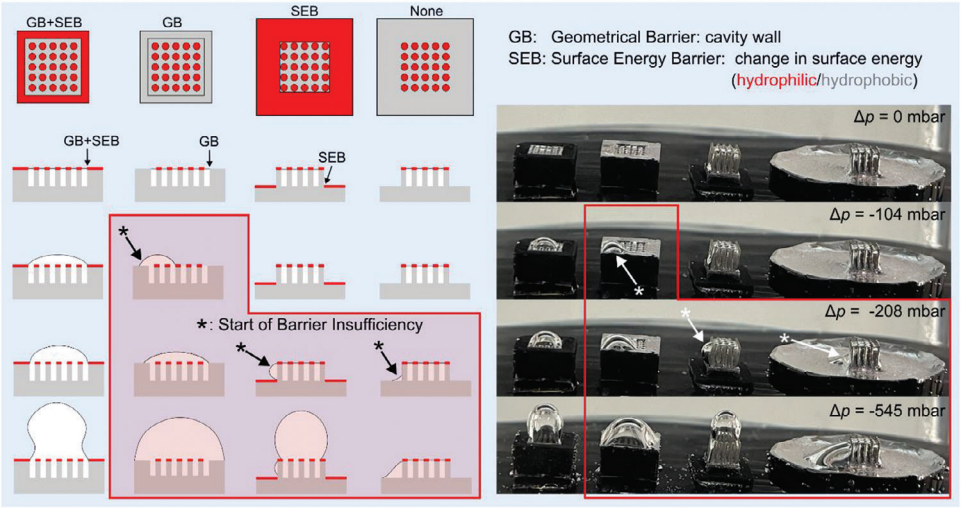

Figure 8. Influence of the geometrical and surface energy barriers: Without a sufficiently bound air volume, the air spring effect cannot increase the stability against under pressure. In this experiment, the barrier of the air volume was modified by changing the sample geometry through removal of the cavity wall we call geometrical barrier (GB), and by reducing the surface energy barrier by omitting the hydrophilic perimeter coating we call surface energy barrier (SEB). The system with both barriers (GB+SEB) performs best, while in case of one or none of the barriers, the system is less stable, and the air starts spreading laterally (marked by *) before bubble detachment would occur. Furthermore, laterally spread bubbles are weaker bound and could easily be displaced, e.g., in hydrodynamic flow conditions, leading to air loss. The air spring effect is therefore only effective in double barrier systems, with both GB and SEB.

parameters, such as pitch or syn-trichome diameter, and surface chemistry, e.g. different coating chemistries. Above all, the thickness of the air spring must be carefully considered when designing artificial air retention structures, especially if pressure fluctuations are to be expected, such as in turbulent flow conditions.

4. Experimental Section

Preparation of Artificial Salvinia-Effect Structures: The master structures were prepared by stereo lithography using a FORMLABS Form 3L System with Grey Resin, with a z-resolution of 25 µm, using self-created CAD files.

These master structures were then replicated first in as-received silicone rubber (Troll Factory Typ 3,Troll Factory), following the manufacturers guidelines. From these new negatives, positive replicates were molded using as-received epoxy resin (epoxy L, hardener L, R&G Faserverbundwerkstoffe GmbH) following manufacturers guidelines.

A hydrophobic coating was prepared by suspending 1 wt% hydrophobically modified fumed silica particles in a 0.5 wt% solution of Teflon AF (Teflon AF 2400X-J, in a perfluorinated solvent (FC770, 3 M) through stirring for 15 minutes.

The samples were submerged in the solution, removed with tweezers and the excess removed through compressed air. After drying, the surface was successfully coated.

For the hydrophilic coating, poly-(4-vinylpyridine) (Polymer Standards Service, Mainz) was dissolved at 3 wt% in ethanol abs. (Ethanol abs., Sigma-Aldrich) under stirring, until all polymer has dissolved. For the coating of the tips, this solution was spread on a piece of soft rubber and the samples stamp onto the rubber. First the samples were stored in plain air, until all solvent had evaporated. Afterwards, the coating was hardened using a homebuilt UV-chamber (lamp type MHL 570, 400 W, 20 min).

Air–Water Interface Differential Pressure Stability Determination: For imaging the air–water interface of submerged structures at variable negative pressures, a self-made pressure cell with an optical window and a sample manipulator was used (Volume: 14 ml). After filling the pressure cell with water, 40 mL of a sonicated aqueous suspension of fluorescent pigment PS10 (Radiant Color N.V., Houthalen, Belgium) was injected. The insoluble pigment particles were sedimented onto the air–water interface within 20 min. After that, the cell was connected to vacuum pump and a 10-liter buffer recipient to apply variable under pressures and overpressures. The fluorescent signal of the decorated air-water interface was imaged using a confocal laser scanning microscope (Leica TCS SP 2 X-1) system with an excitation wavelength of 458 nm and 488 nm and HC PL Fluotar 5 × /0.15 POL Leica 5x dry objective.

After changing the pressure in the recipient, the valve separating the cell from this recipient was open, thus immediately changing the pressure in the cell. If the pressure was below the snap off pressure, the snap off occurred instantaneously. The chosen pressure was held over a period of about 5 min, the required scanning time. The duration of pressure application did not influence the air-water-interface (tested up to 1 h).

For a determination of the required pressure, at first a rough approach in 50 mbar steps was chosen. In subsequent measurements, further increments of up to 5 mbar steps were used.

Additionally, for the determination of the snap off pressure, the samples were submerged in the pressure cell and the air water interface was observed, while continuously lowering the pressure at a rate of about 10 mbar s^{-1} until a snap-off was observed. After the snap-off, the pressure was returned to atmospheric pressure at the same rate, thus ensuring equal contact of the interface with all pillars.

To demonstrate the varying behavior at identical under pressure, multiple samples were concurrently submerged in a larger pressure vessel (Volume: 1.2 L) as the pressure difference was continuously increased beyond snap of pressure of the most stable structure while the interfaces were documented using a camera.

Acknowledgements

The authors acknowledge financial support by the German Ministry of Education and Research, BMBF project ARES, the Baden-Wuerttemberg Stiftung and by the European Commission (EC) within the H2020project AIRCOAT (Air Induced friction Reducing ship Coating). The authors also acknowledge the earlier contributions of members of our research group in Karlsruhe at KIT (Aaron Weis) and Dr. Matthias Mail support with SEM investigations of the surface. The authors further acknowledge the support

by the Karlsruhe Micro and Nano Facility (KNMFi) Project-ID: 2018-021-025049.

Open access funding enabled and organized by Projekt DEAL.

Conflict of Interest

The authors declare no conflict of interest.

Data Availability Statement

The data that support the findings of this study are available from the corresponding author upon reasonable request.

Keywords

air spring effect, biomimetics, *Salvinia* effect, superhydrophobicity, underwater air retention

Received: June 12, 2024
Published online:

[1] W. Barthlott, T. Schimmel, S. Wiersch, K. Koch, M. Brede, M. Barczewski, S. Walheim, A. Weis, A. Kaltenmaier, A. Leder, H. F. Bohn, *Adv. Mater.* **2010**, *22*, 2325.
[2] W. Barthlott, C. Neinhuis, *Planta*. **1997**, *202*, 1.
[3] C. Neinhuis, *Ann. Bot.* **1997**, *79*, 667.
[4] R. Blossey, *Nat. Mater.* **2003**, *2*, 301.
[5] M. Callies, D. Quéré, *Soft Matter.* **2005**, *1*, 55.
[6] P. Roach, N. J. Shirtcliffe, M. I. Newton, *Soft Matter.* **2008**, *4*, 224.
[7] W. Barthlott, M. Mail, C. Neinhuis, *Philos. Trans. R. Soc., A.* **2016**, *374*, 20160191.
[8] W. Barthlott, M. D. Rafiqpoor, W. R. Erdelen, in *Biomimetic Research for Architecture and Building Construction: Biological Design and Integrative Structures* (Eds: J. Knippers, K. G. Nickel, T. Speck), Vol. *8*, Springer International Publishing, Berlin **2016**, pp. 11–55.
[9] Y. Y. Yan, N. Gao, W. Barthlott, *Adv. Colloid Interface Sci.* **2011**, *169*, 80.
[10] Y. Sun, Z. Guo, *Nanoscale Horiz.* **2019**, *4*, 52.
[11] Y. Si, Z. Dong, L. Jiang, *ACS Cent. Sci.* **2018**, *4*, 1102.
[12] M. Mail, A. Klein, H. Bleckmann, A. Schmitz, T. Scherer, P. T. Rühr, G. Lovric, R. Fröhlingsdorf, S. N. Gorb, W. Barthlott, *Beilstein J. Nanotechnol.* **2018**, *9*, 3039.
[13] J. Ou, B. Perot, J. P. Rothstein, *Phys. Fluids.* **2004**, *16*, 4635.
[14] G. McHale, N. J. Shirtcliffe, C. R. Evans, M. I. Newton, *Appl. Phys. Lett.* **2009**, *94*, 064104.
[15] A. K. Balasubramanian, A. C. Miller, O. K. Rediniotis, *AIAA J.* **2004**, *42*, 411.
[16] N. J. Shirtcliffe, G. McHale, M. I. Newton, Y. Zhang, *ACS Appl. Mater. Interfaces.* **2009**, *1*, 1316.
[17] G. McHale, M. I. Newton, N. J. Shirtcliffe, *Soft Matter.* **2010**, *6*, 714.
[18] H. Dong, M. Cheng, Y. Zhang, H. Wei, F. Shi, *J. Mater. Chem. A.* **2013**, *1*, 5886.
[19] W. T. Rong, H. F. Zhang, Z. G. Mao, X. W. Liu, K. G. Song, *Mater. Res. Express.* **2020**, *7*, 015092.
[20] M. N. Kavalenka, F. Vülliers, S. Lischker, C. Zeiger, A. Hopf, M. Röhrig, B. E. Rapp, M. Worgull, H. Hölscher, *ACS Appl. Mater. Interfaces.* **2015**, *7*, 106515.
[21] M. C. Xu, A. Grabowski, N. Yu, G. Kerezyte, J. W. Lee, B. R. Pfeifer, C. J. Kim, *Phys. Rev. Appl.* **2020**, *13*, 034056.
[22] Y. C. Jung, B. Bhushan, *J. Phys.: Condens. Matter.* **2010**, *22*, 035104.
[23] C.-H. Choi, C.-J. Kim, *Phys. Rev. Lett.* **2006**, *96*, 066001.
[24] C. Lee, C.-H. Choi, C.-J. C. Kim, *Phys. Rev. Lett.* **2008**, *101*, 064501.
[25] F. Feuillebois, M. Z. Bazant, O. I. Vinogradova, *Phys. Rev. Lett.* **2009**, *102*, 026001.
[26] K. Koch, H. F. Bohn, W. Barthlott, *Langmuir.* **2009**, *25*, 141160.
[27] B. Bhushan, Y. C. Jung, *Prog. Mater. Sci.* **2011**, *56*, 1.
[28] J. Breveleri, S. Mohammadshahi, T. Dunigan, H. Ling, *Colloids Surf., A.* **2023**, *676*, 132319.
[29] H. Park, C.-H. Choi, C.-J. Kim, *Exp. Fluids.* **2021**, *62*, 229.
[30] B. Bhushan, *Beilstein J. Nanotechnol.* **2011**, *2*, 66.
[31] J. Busch, W. Barthlott, M. Brede, W. Terlau, M. Mail, *Philos. Trans. R. Soc., A.* **2019**, *377*, 20180263.
[32] B. Bhushan, *Biomimetics:Bioinspired Hierarchical-Structured Surfaces for Green Science and Technology*, Vol. *279*, Springer International Publishing, Cham, Switzerland **2018**.
[33] M. Liravi, H. Pakzad, A. Moosavi, A. Nouri-Borujerdi, *Prog. Org. Coat.* **2020**, *140*, 105537.
[34] L. Xin, H. Li, J. Gao, Z. Wang, K. Zhou, S. Yu, *Friction.* **2023**, *11*, 716.
[35] C. W. Judith Geils, A. Baars, A. Kesel, M. Beltri, S. Larroze, V. Schneider, Herbert, J. O. Bretschneider, S. Walheim, T. Schimmel, *EU Aircoat S1 Test report*, **2019**, https://cordis.europa.eu/project/id/764553/results, (accessed: September 2024).
[36] A. Solga, Z. Cerman, B. F. Striffler, M. Spaeth, W. Barthlott, *Bioinspiration Biomimetics.* **2007**, *2*, S126.
[37] X. Sheng, J. Zhang, *Colloids Surf., A.* **2011**, *377*, 374.
[38] M. A. Samaha, H. V. Tafreshi, M. Gad-el-Hak, *C. R. Mec.* **2012**, *340*, 18.
[39] J. Hunt, B. Bhushan, *J. Colloid Interface Sci.* **2011**, *363*, 187.
[40] C. Lee, C.-J. C. J. Kim, *Langmuir.* **2009**, *25*, 128128.
[41] M. Röhrig, M. Mail, M. Schneider, H. Louvin, A. Hopf, T. Schimmel, M. Worgull, H. Hölscher, *Adv. Mater. Interfaces.* **2014**, *1*, 1300083.
[42] F. Vüllers, Y. Germain, L. M. Petit, H. Hölscher, M. N. Kavalenka, *Adv. Mater. Interfaces.* **2018**, *5*, 1800125.
[43] F. Vüllers, S. Peppou-Chapman, M. N. Kavalenka, H. Hölscher, C. Neto, *Phys. Fluids.* **2019**, *31*, 012102.
[44] W. Konrad, C. Apeltauer, J. Frauendiener, W. Barthlott, A. Roth-Nebelsick, *J. Bionic Eng.* **2009**, *6*, 350.
[45] M. Xu, G. Sun, C.-J. Kim, *Phys. Rev. Lett.* **2014**, *113*, 136103.
[46] A. Marmur, S. Kojevnikova, *J. Colloid Interface Sci.* **2020**, *568*, 148.
[47] M. Mail, S. Walheim, T. Schimmel, W. Barthlott, S. N. Gorb, L. Heepe, *Beilstein J. Nanotechnol.* **2022**, *13*, 1370.
[48] Y. L. Xiang, S. L. Huang, P. Y. Lv, Y. H. Xue, Q. Su, H. L. Duan, *Phys. Rev. Lett.* **2017**, *119*, 134501.
[49] W. Barthlott, M. Mail, B. Bhushan, K. Koch, *Nano-Micro Lett.* **2017**, *9*, 23.
[50] M. J. Mayser, H. F. Bohn, M. Reker, W. Barthlott, *Beilstein J. Nanotechnol.* **2014**, *5*, 812.
[51] M. Moosmann, T. Schimmel, W. Barthlott, M. Mail, *Beilstein J. Nanotechnol.* **2017**, *8*, 1671.
[52] O. Tricinci, T. Terencio, B. Mazzolai, N. M. Pugno, F. Greco, V. Mattoli, *ACS Appl. Mater. Interfaces* **2015**, *7*, 25560.
[53] O. Tricinci, T. Terencio, N. M. Pugno, F. Greco, B. Mazzolai, V. Mattoli, *Micromachines.* **2017**, *8*, 366.
[54] Y. Xiang, S. Huang, T.-Y. Huang, A. Dong, D. Cao, H. Li, Y. Xue, P. Lv, H. Duan, *Proc. Natl. Acad. Sci. USA.* **2020**, *117*, 2282.
[55] C.-Y. Yang, C.-Y. Yang, C.-K. Sung, *Jpn. J. Appl. Phys.* **2013**, *52*, 06GF08.
[56] M. Mail, M. Moosmann, P. Häger, W. Barthlott, *Philos. Trans. R. Soc., A.* **2019**, *377*, 20190126.
[57] Y. Zheng, X. Zhou, Z. Xing, T. Tu, *Text. Res. J.* **2019**, *89*, 2859.
[58] M. J. Mayser, W. Barthlott, *Integr. Comp. Biol.* **2014**, *54*, 1001.
[59] R. Poetes, K. Holtzmann, K. Franze, U. Steiner, *Phys. Rev. Lett.* **2010**, *105*, 166104.

[60] Y. Zheng, X. Zhou, Z. Xing, T. Tu, *RSC Adv.* **2018**, *8*, 10719.
[61] K. Zhou, D. Li, P. Xue, P. Wang, Y. Zhao, M. Jin, *Colloids Surf. A.* **2020**, *590*, 124517.
[62] M. Kim, S. Yoo, H. E. Jeong, M. K. Kwak, *Nat. Commun.* **2022**, *13*, 5181.
[63] A. B. Tesler, S. Kolle, L. H. Prado, I. Thievessen, D. Böhringer, M. Backholm, B. Karunakaran, H. A. Nurmi, M. Latikka, L. Fischer, S. Stafslien, Z. M. Cenev, J. V. I. Timonen, M. Bruns, A. Mazare, U. Lohbauer, S. Virtanen, B. Fabry, P. Schmuki, R. H. A. Ras, J. Aizenberg, W. H. Goldmann, *Nat. Mater.* **2023**, *22*, 1548.
[64] W. Barthlott, S. Wiersch, Z. Čolić, K. Koch, *Botany.* **2009**, *87*, 830.
[65] W. Barthlott, E. Wollenweber, Zur Feinstruktur Chemie und taxonomischen Signifikanz epicuticularer Wachse und ähnlicher Sekrete **1981**, *32*, http://www.lotus-salvinia.de/pdf/038, (accessed: September 2024).
[66] D. Gandyra, S. Walheim, S. Gorb, P. Ditsche, W. Barthlott, T. Schimmel, *Small.* **2020**, *16*, 2003425.
[67] M. Amabili, A. Giacomello, S. Meloni, C. M. Casciola, *Adv. Mater. Interfaces.* **2015**, *2*, 1500248.
[68] O. Tricinci, F. Pignatelli, V. Mattoli, *Adv. Funct. Mater.* **2023**, *33*, 2206946.
[69] Y. Zhang, Y. Hu, B. Xu, J. Fan, S. Zhu, Y. Song, Z. Cui, H. Wu, Y. Yang, W. Zhu, F. Wang, J. Li, D. Wu, J. Chu, L. Jiang, *ACS Nano.* **2022**, *16*, 2730.